Effect of processing on microstructural features and mechanical properties of a reduced activation ferritic/martensitic EUROFER steel grade

Puype, A.; Malerba, L.; De Wispelaere, N.; Petrov, R.; Sietsma, J.

DOI
10.1016/j.jnucmat.2017.07.001

Publication date
2017

Document Version
Accepted author manuscript

Published in
Journal of Nuclear Materials

Citation (APA)
Puype, A., Malerba, L., De Wispelaere, N., Petrov, R., & Sietsma, J. (2017). Effect of processing on microstructural features and mechanical properties of a reduced activation ferritic/martensitic EUROFER steel grade. *Journal of Nuclear Materials*, *494*, 1-9. https://doi.org/10.1016/j.jnucmat.2017.07.001

Link to formal publication Journal of Nuclear Materials (Elsevier): https://doi.org/10.1016/j.jnucmat.2017.07.001

Effect of Processing on Microstructural Features and Mechanical Properties of a Reduced Activation Ferritic/Martensitic EUROFER Steel Grade

A. Puype[1*], L. Malerba[3], N. De Wispelaere[4], R. Petrov[1,2], J. Sietsma[1,2]

[1] Department of Materials Science and Engineering, Ghent University, Technologiepark 903, B-9052 Zwijnaarde

[2] Department of Materials Science and Engineering, TU-Delft, Mekelweg 2, NL-2628 CD Delft, The Netherlands

[3] SCK·CEN, Boeretang 200, B-2400 Mol

[4] OCAS, Technologiepark 903, B-9052 Zwijnaarde

Abstract

The microstructure of a 9Cr-1W-0.22V-0.09Ta-0.11C reduced activation ferritic/martensitic (RAFM) steel has been investigated after thermo-mechanical rolling with subsequent annealing for 30 min at temperatures of 880°C, 920°C, 980°C and 1050°C, followed by water quenching. Scanning and transmission electron microscopy investigations and electron backscattered diffraction (EBSD) measurements were performed to determine the microstructural features after the different thermal treatments. Additionally, the microstructure and the mechanical properties of the materials were studied after tempering at 750°C for 2 hours. This study aims to understand microstructural processes that occur in the material during thermo-mechanical treatment and to assess the effect of the microstructure on its strength and toughness, with a view on improving its

mechanical performance. Microstructural analysis together with the data from mechanical tests identified the beneficial effect of grain refinement obtained with adequate processing on the ductile-to-brittle transition temperature (DBTT) and on the delay of strength degradation at elevated temperatures.

1. Introduction

Recently, the European Fusion Development Agreement (EFDA) released a roadmap for the realization of nuclear fusion energy for electricity production [1]. Currently, the construction of the International Thermonuclear Experimental Reactor (ITER) facility is ongoing to acquire knowledge and test technologies necessary for the design and realization of a thermonuclear fusion power plant for electricity production by the mid-21st century. Simultaneously, leading-edge fusion-related research focuses on the development of structural materials for first wall components and tritium breeding blankets in the future DEMO (demonstration fusion) reactor [2-5]. These structural materials will have to face much higher temperatures and neutron doses in comparison with in-service conditions of current fission reactors [6]. Consequently, new materials need to be developed or current structural materials need to be adapted for more severe working conditions.

EUROFER97, a reduced activation ferritic/martensitic (RAFM) 9%Cr steel, is currently selected in the European fusion program as the reference structural material for the fusion breeding blanket. The composition of RAFM steel grades has been modified in comparison with commercial 9Cr-1Mo steels, by replacing high activation alloying elements like Mo, Nb, Ni and Co with low activation Ta, W and V for easier nuclear waste disposal. This material shows good performance in the operational temperature range of 350-550°C [7, 8]. It is however desirable to widen this operating window. The lower bound of the service temperature is defined by radiation-

induced embrittlement. The lower limit of the operation temperature may be further reduced below 350°C by decreasing the ductile-to-brittle transition temperature (DBTT) before irradiation. This may prevent the shift of DBTT to temperatures higher than room temperature during operation. The upper limit of the service temperature, on the other hand, is determined by the creep resistance. Improvement of the stability of the microstructure at high temperature may allow working at temperatures higher than 550°C.

By standard, plates of RAFM steels such as EUROFER97 are produced by forging, followed by one or two hot rolling steps at fixed temperature (i.e. conventional hot rolling). The plate material obtains its functional properties by a two-stage heat treatment, which consists of an annealing stage in the austenitic region, followed by quenching and tempering stage [9]. This thermal treatment creates a microstructure of tempered martensite with specific distribution characteristics of $M_{23}C_6$ and MX precipitates, which significantly affect the mechanical properties. Martensite in RAFM steels shows a hierarchical microstructure where packets are confined within prior austenite grains (PAG). A packet consists of blocks with common habit plane. In turn, each block is a group of laths with the same crystal orientation, i.e. the same variant [10, 11]. When the material is tempered at 760°C for 2 hours, recovery of the dislocation structure occurs and the laths form elongated subgrains [12]. It has been shown by Dossett *et al.* [13] that significant and cost-effective improvements in the final properties of ferritic/martensitic (FM) steel can be obtained by controlling the microstructure during processing. Especially in recent years, researchers discussed the positive effect of a thermo-mechanical (TM) treatment like ausforming on the microstructure and mechanical properties of stainless steels [14], FM steels [15, 16] and also RAFM steels [17]. There is consensus on the fact that the size of martensite units (blocks, packets) correlates with the austenite grain size and with the strain

applied during work-hardening in the austenite region, i.e. during repeated hot rolling at decreasing temperature [18, 19]. This TM-rolling modifies the austenite condition by deformation before transformation to martensite. The deformation of austenite induces the formation of dislocation substructures within the austenitic grains. The accumulated strain in austenite induces an increased dislocation density in the martensitic structure during transformation. In other words, the grain substructure with increased defect dislocation density in work-hardened austenite has an influence on the austenite-martensite transformation and on the precipitation reactions in the transformation product [20]. The TM-rolled microstructure before annealing consists of heavily distorted elongated martensite, due to the treatment received in the austenitic region. It has been shown that vanadium slows down the static softening kinetics of the austenite and therefore retards the austenite recrystallization during TM-treatment [21]. Yada *et al.*[22] and Dossett *et al.*[13] also found that the presence of minimum concentrations of alloying elements such as tantalum and vanadium are particularly useful to retard the recrystallization and grain coarsening by controlled precipitation during annealing. The high density of defects, especially dislocations, as inheritance from the parent phase provides abundant nucleation sites for phase transformation, resulting in very fine austenitic grains upon heating during the annealing stage. The deformed austenitic grain structure with high defect density after TM-rolling results in a similar way in a grain refinement in water quenched condition, as compared to water quenched material obtained from the initial equiaxed martensitic structure after conventional hot rolling, like for EUROFER97-2.

This reference material, EUROFER97-2, consists of a lath martensitic structure with a high dislocation density in quenched condition after annealing above $A_{c3,}$ at 980°C, for 30 min. The critical transformation temperatures for EUROFER97 are reported as A_{c1} = 820°C and A_{c3} =

890°C, but the applied heating rates are not defined [23]. The quenched and tempered (Q&T) RAFM steel exhibits a tempered martensitic structure with Cr and W-rich coarse $M_{23}C_6$ carbides with size distribution in the range of 60-150 nm, on prior austenite, packet and block grain boundaries, as well as small Ta- or V-rich MX carbonitrides with average size of 20-80 nm, finely distributed in the interior lath structure. $M_{23}C_6$ carbides partially stabilize the boundaries, while the MX particles pin the dislocations, retarding the annihilation of dislocations in the martensite (recovery of the martensite) during high temperature exposure. The strength of RAFM steels stems from solid-solution strengthening, dislocation-particle interactions, dislocation-dislocation interactions, and dislocation-boundary interactions [12].

The mechanical degradation after long-term exposure at high temperature stems from coarsening of the precipitates and extended recovery of the martensitic structure [24, 25]. A better high temperature response of RAFM steels could extend the current operating temperature window of RAFM steels. Therefore, the goal of the current work is to develop different microstructures by thermo-mechanical treatments and to investigate the correlation between microstructure and high temperature properties of a lab-cast EUROFER grade for tritium breeding module test applications in ITER and for first wall structural material in DEMO.

2. Experimental

2.1 Material, hot rolling and thermal treatment

The chemical composition of the lab-cast EUROFER grade is shown in Table 1, together with the compositional range of EUROFER97-2 for comparison. The cast weighed 60 kg with dimensions of ± 300 x 250 x 125 mm³. A slab with dimensions of 126 x 120 x 70.6 mm³ was cut off and rolled to a plate with a final thickness of 11 mm. Specifically, the lab-cast EUROFER was heated

to a temperature of 1250 °C for one hour after which it was rolled in 6 rolling passes at pre-defined decreasing temperatures of 1200 °C, 1150 °C, 1100 °C, 960 °C, 900°C and a final rolling temperature (FRT) of 850 °C with a reduction of 20-30% per pass. After these temperature-controlled rolling steps, the thermo-mechanically (TM) rolled slab was air cooled to room temperature.

Table 1: Chemical composition of EUROFER97-2 [7] and lab-cast EUROFER grade.

[wt%]	C	Si	Mn	P	S	N	V	Ta	W	Cr	Fe
EU97-2	0.09-0.12	0.05	0.2-0.6	0.005	0.005	0.015-0.045	0.15-0.25	0.10-0.14	1-1.2	8.5-9.5	Bal.
Lab-cast EUROFER	0.11	0.038	0.40	0.0023	0.0029	0.011	0.22	0.086	1.0	9.3	Bal.

Eight plates with dimensions of 25 x 25 x 10 mm³ and four plates with dimensions of 100 x 50 x 10 mm³ were cut out of the TM rolled slab for microstructural characterization and mechanical testing, respectively. A full schematic representation of the performed processing steps is presented in Fig. 1. The plates were heat treated in the furnace with temperature control by thermocouples type K with an accuracy of 7°C. The material was annealed at four different temperatures (T_{anneal}) 880°C, 920°C, 980°C and 1050°C and subsequently water quenched. Four 25 x 25 x 10 mm³ plates were characterized in the quenched state from the four mentioned temperatures: they will be denoted from now on as water quenched (WQ) material (Fig. 1).

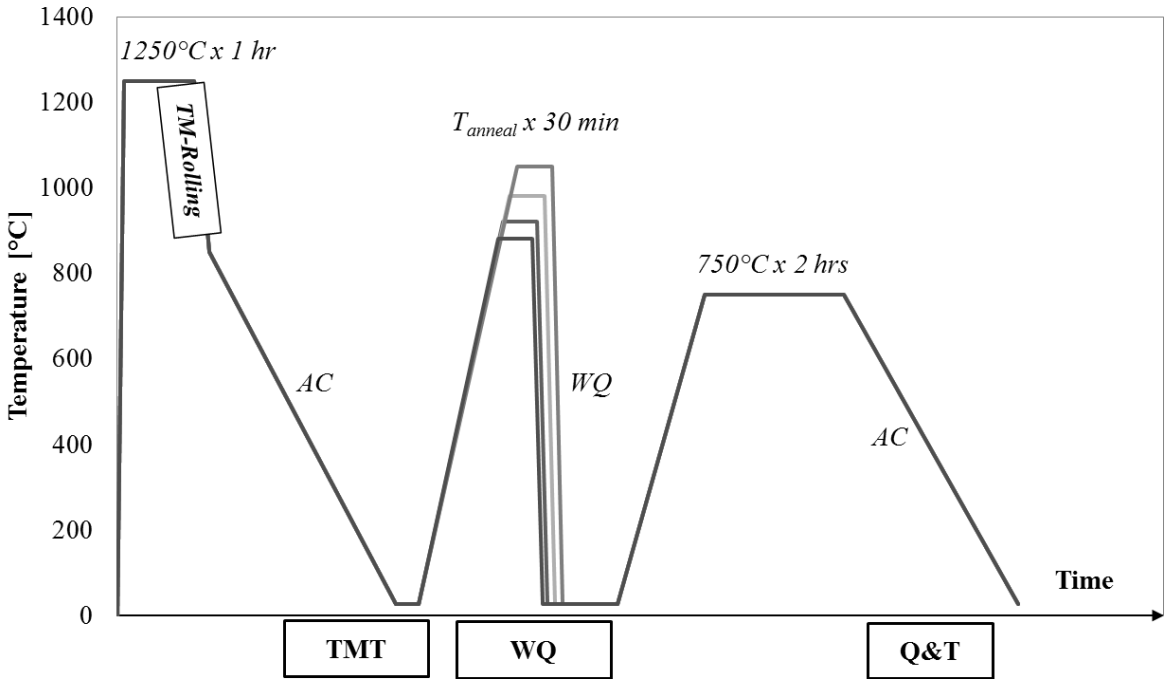

Fig. 1: Schematic representation of the TM rolling followed by air cooling (TMT) and heat treatment with variable Tanneal =880°C, 920°C, 980°C and 1050°C for 30 min. followed by water quenching (WQ) and tempering at 750°C for 2 hrs. (Q&T).

The four other 25 x 25 x 10 mm³ WQ materials and the plates for mechanical testing were subsequently tempered at 750°C for 2 hours, and air cooled. These materials will be further denoted as quenched and tempered (Q&T) samples (Fig. 1).

2.2 Microstructural characterization

The microstructure of the WQ and Q&T samples was investigated with optical microscopy (OM) and scanning electron microscopy (SEM) after metallographic sample preparation. Mechanical grinding and polishing up to 1 µm diamond suspension, and subsequent etching with Vilella's reagent (1 gr picric acid + 5 ml hydrochloric acid + 100 ml ethanol) was applied to all samples. SEM analysis was made with a FEI Quanta^{TM} 450-FEG-SEM. Specimens for electron backscattered diffraction (EBSD) analysis were metallographically prepared up to a polishing step of 1 µm diamond paste. An additional polishing step for 30 minutes with a 35 nm colloidal

silica suspension was performed afterwards. EBSD patterns were acquired on a FEI Quanta™ 450-FEG-SEM equipped with a Hikari detector operated with EDAX-TSL OIM-Data Collection version 6.2® software. The analysis was performed with an acceleration voltage of 20 kV, working distance of 16 mm, tilt angle of 70° and step size of 25 nm in a hexagonal grid. The orientation data were post-processed with EDAX-TSL OIM™ data analysis software.

Data analysis of EBSD measurements was performed to determine microstructural characteristics like PAG size, martensitic block size and lath thickness. High resolution to resolve single martensitic laths was ensured by using a step size of 25 nm. To avoid the incorporation of misinterpreted pixels during data analysis, only laths greater than an area of 5 pixels were considered. An hexagonal grid was chosen for better statistics of the misorientation of neighboring points.

For the evaluation of the lath dimensions, misorientations were calculated for every pixel-neighbor combination. If the misorientation is less than 1°, the two points were interpreted as belonging to the same lath [26]. Thus, to measure the lath thickness, a grain definition of minimum misorientation angle of 1° was used, before calculating the average area fraction of the grains. The applied grain definition for a martensitic block, proposed by Morito [11], defines a minimum misorientation angle of 15°. The effective martensitic block size is defined here as the equivalent diameter of the area enclosed by high angle grain boundaries (misorientation angle larger than 15°).

In order to determine the precipitated fraction of V, Ta and Cr within the steel matrix, electrolysis of the samples was done to dissolve the steel matrix whilst keeping the precipitates unaffected. Afterwards, the electrolyte was filtered to separate the precipitates. After filtration, the filters (containing the precipitates) were dissolved by microwave stimulation and analyzed by

inductively coupled plasma mass spectroscopy (ICP-MS) to determine the precipitated fraction of V, Ta and Cr. The solvent of the organic phase was analyzed with inductively coupled plasma optical emission spectrometry (ICP-OES).

For transmission electron microscopy, 3-mm diameter discs were punched out from thin foils and subsequently subjected to twin jet electropolishing, using a mixture of electrolyte of 90 % acetic acid and 10 % perchloric acid. The thin electron transparent samples were examined in a transmission electron microscope (JEOL 3010 STEM) at 300 kV operating voltage. TEM diffraction and energy dispersive spectroscopy (EDS) were used to determine the crystal structure and composition of the observed particles. Additionally, ImageJ was used to analyse the size distribution of the particles.

2.3 Mechanical testing

Hardness measurements were carried out on a Zwick Hardness tester with a load of 50 N (5 kgf, HV5) after grinding and polishing up to 1 μm diamond suspension. The average of 10 hardness measurements was taken along the length of the sample.

Tensile specimens with L-T orientation were prepared from the 100 x 50 x 10 mm^3 Q&T plates. The tensile specimens have a 15 mm gauge length, and a width and thickness of 3 mm. Tensile testing was carried out in a 50 kN load-capacity tensile testing machine following ASTM standard E8-E8M [27]. Displacement controlled tests at cross-head speed of 0.2 mm/min ($\dot{\varepsilon} \approx 2 * 10^{-4} s^{-1}$) were carried out at -50°C, 23°C, 200°C, 400°C, 550°C, 650°C, 750°C and 850°C.

Charpy V notch impact testing of KLST (Kleinstprobe)-type miniaturized MCVN specimens with L-T orientation was performed on a CEAST machine at temperatures ranging between -150°C and room temperature.

3. Results and discussion

3.1 Microstructural characterization

The WQ materials have a martensitic structure irrespective of the annealing temperature. However, the grain features do depend on the annealing temperature. The grains of the WQ materials are represented in Fig. 2 by unique grain colour maps obtained with EBSD, where an arbitrary color is attributed to each martensitic block (Fig. 2). The grain definition is set to a minimum misorientation angle of 15°, a minimum of 5 pixels/grain and minimum confidence index (CI) of 0.1. It should be noted that the transformation temperatures were experimentally determined by analysis of dilatometric curves, i.e. as the temperatures where the dilatometric curve deviates for the slope. The critical temperatures for our material, obtained with heating rates of 3°C/s, are A_{c1} = 835°C and A_{c3} = 905°C. These values are slightly higher than the critical temperatures for EUROFER97 obtained by Rieth *et al.*, due to the direct dependence of the measured transformation temperatures on the applied heating rate [28]. Fig. 2 clearly shows that the higher the annealing temperature, the larger the martensitic blocks.

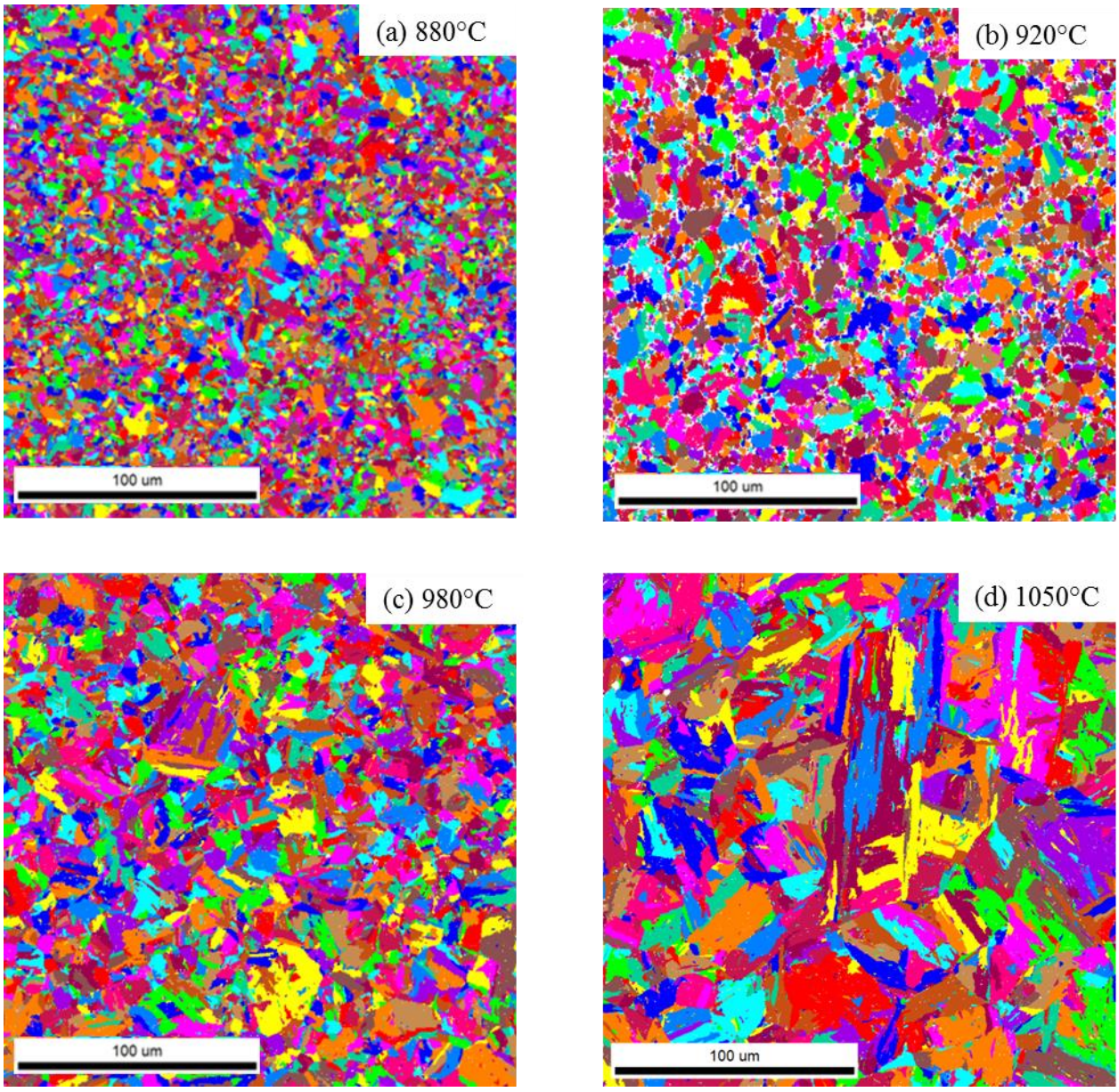

Fig. 2: Unique grain color maps in WQ conditions with annealing temperature of (a) 880°C, (b) 920°C, (c) 980°C and (d) 1050°C.

The dependence of the average martensitic block size on annealing temperature is shown in Fig. 3. The average equivalent block diameter increases as the annealing temperature increases above A_{c3}. Intercritical heating between A_{c1} and A_{c3} renders a small average equivalent block diameter size of 4 ± 1 μm (Fig. 2 (a)). Supercritical annealing above A_{c3} results in martensitic block sizes of 7 ± 2 μm, 8 ± 2 μm and 17 ± 4 μm for annealing temperatures of 920°C, 980°C and 1050°C,

respectively (Fig. 3). The grain size dependence on annealing temperature of the lab-cast material (Fig. 3, black dotted curve) increases progressively compared to the linear dependence of the grain size of EUROFER97-2 on the annealing temperature (Fig. 3, grey dotted curve) [7].

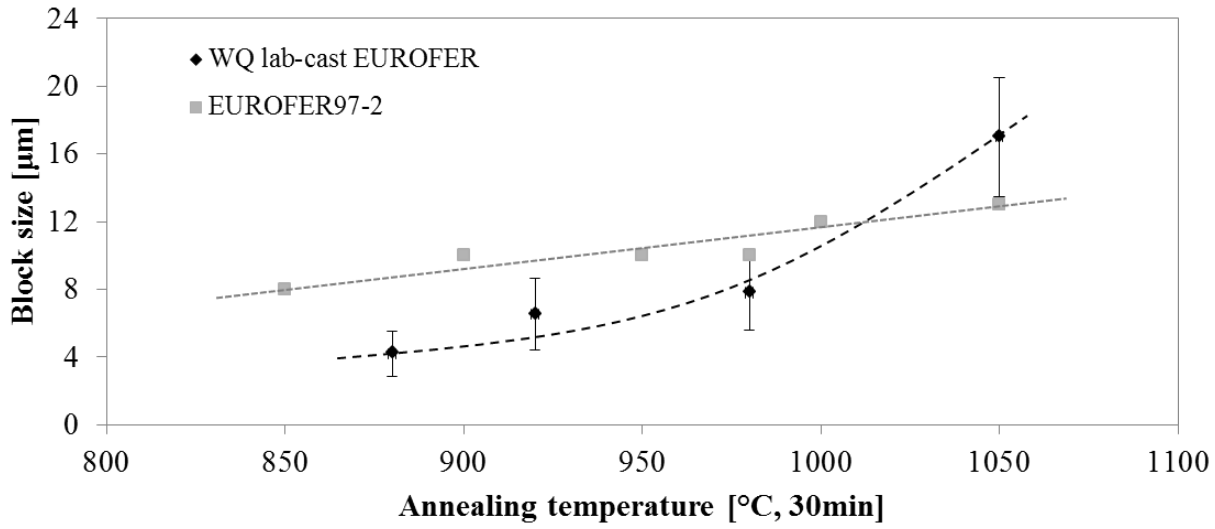

Fig. 3: Black symbols: average martensite block size measurements obtained via orientation imaging microscopy (OIM^{TM}) data analysis for lab-cast EUROFER, with standard error, compared with grain size data available for EUROFER97-2 given by the grey symbols [7].

Increasing the annealing temperature promotes grain growth of the prior austenite grains (PAG) which is due to the reduced impeding action of the precipitated carbonitrides which will be discussed in the next paragraph, as well as to the intrinsic dependence of growth kinetics on temperature, determined by the corresponding activation energy of the process. The coarsening of the PAG becomes extensive above A_{c3}, at temperatures around 1050°C, which is reflected by the large block size (Fig. 2 (d) & Fig. 3). The rapid austenitic grain growth at temperatures around 1050°C is in agreement with the observation of K.S. Chandravathi *et al.* [29].

The tempering step at 750°C for 2 hours was performed on all WQ materials. This heat treatment is also the standard tempering step applied to the reference material. The SEM images of the Q&T microstructures are presented in Fig. 4. The Q&T materials exhibit lath martensitic

morphology. Coarse $M_{23}C_6$ precipitates are observed on the PAG boundaries and packet boundaries after tempering in the case of heat treatment Q(880°C)&T (Fig. 4 (a)). As the annealing temperature of the Q&T treatment increases to 920°C and 980°C, finer $M_{23}C_6$ precipitates are found on the PAG boundaries and packet boundaries with additional precipitation of $M_{23}C_6$ occurring on the block boundaries as well (Fig. 4 (b) & (c)). The microstructure after heat treatment Q(1050°C)&T contains coarser $M_{23}C_6$, in comparison with the microstructures after Q(920°C)&T and Q(980°C)&T, located on PAG boundaries, packet boundaries and block boundaries (Fig. 4 (d)).

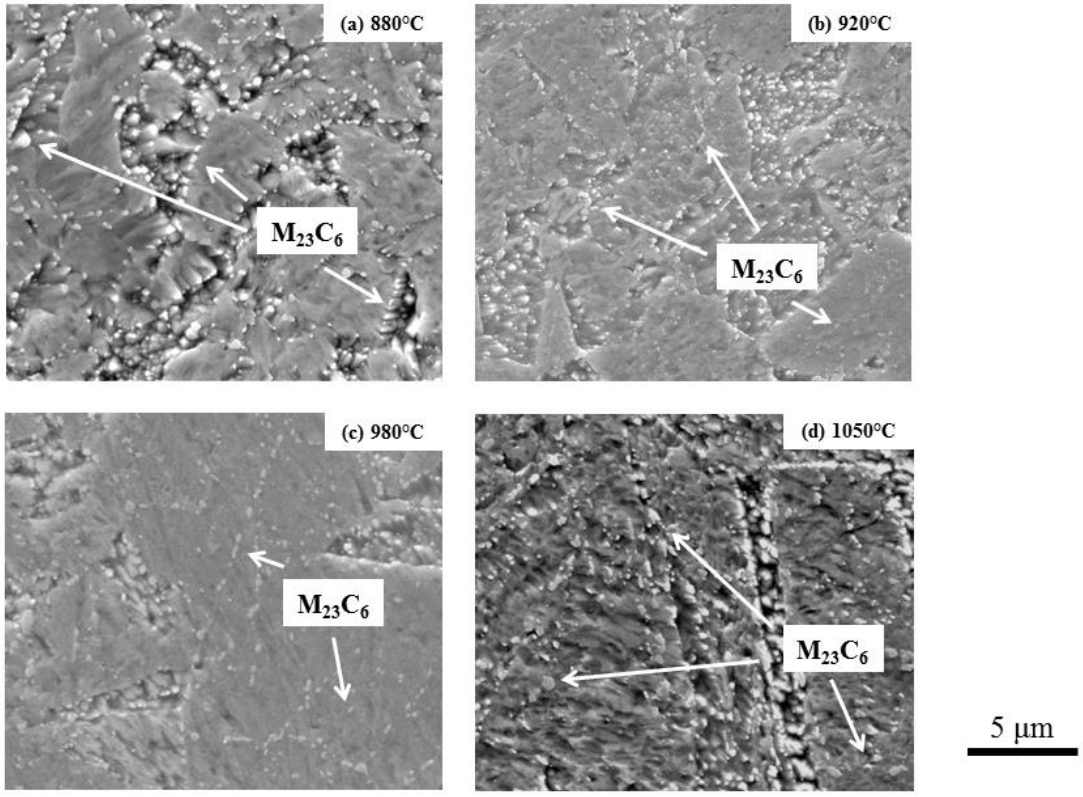

Fig. 4: SEM images of material in Q&T condition after different annealing temperatures (a) 880°C, (b) 920°C, (c) 980°C and (d) 1050°C.

Inductively coupled plasma mass spectroscopic (ICP-MS) investigations reveal the fraction of carbonitrides in the matrix after TM-rolling, water quenching (WQ) (Fig. 5) and Q&T treatment (Fig. 6). Clearly, after TM-rolling most of the vanadium and tantalum remains in solid solution, even after air cooling from the final rolling temperature (850°C) to room temperature (Fig. 5 TMT), as also observed by A.A. Barani *et al.* [20] in TM treated Si-Cr-V steel. It is expected that a work-hardened austenitic state reduces the grain boundary segregation of V, Ta and other alloying elements by offering preferential segregation sites or traps like dislocation substructures or vacancies within the austenite grains. This reduces the diffusion of these elements towards the grain boundaries and retards nucleation of precipitates on the boundaries by redistribution of the elements inside the grains. During annealing, small fractions of carbides and carbonitrides do precipitate on grain boundaries and inside the lath interior, respectively, in different quantities depending on the annealing temperature.

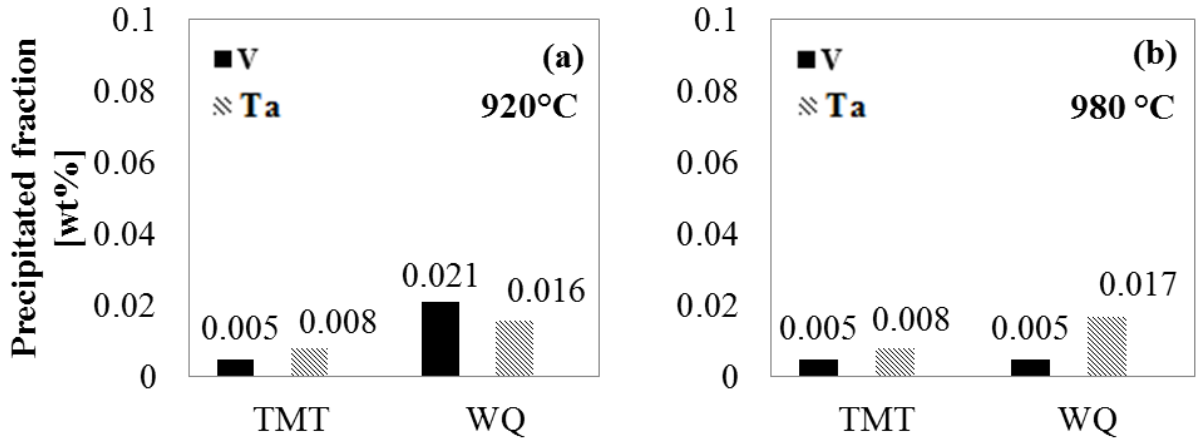

Fig. 5: ICPMS results; fraction of MX precipitates after TMT and as-quenched (WQ) for annealing temperature of 920°C (a) and 980°C (b). The estimated uncertainty is 0.005 wt%.

Equilibrium thermodynamic calculations, using Thermo-Calc 2016 database TCFE7, show that the dissolution temperatures of $M_{23}C_6$ carbides and carbonitrides (V,Ta)N and TaC for our lab-cast EUROFER grade are 898°C, 987°C and 1166°C, respectively. At intercritical annealing below A_{c3} (annealing temperature of 880°C), which is also below the dissolution temperature of the three classes of precipitates, $M_{23}C_6$ carbides, and (V,Ta)N and TaC carbonitrides are formed. The coarse $M_{23}C_6$ carbides on the PAG boundaries (Fig. 4 (a)) imply precipitation during annealing at 880°C. At higher annealing temperatures, the size and fraction of precipitated $M_{23}C_6$ on the PAG boundaries decreases, and the fraction of $M_{23}C_6$ on packet and block boundaries increases (Fig. 4 (b), (c) & (d)).

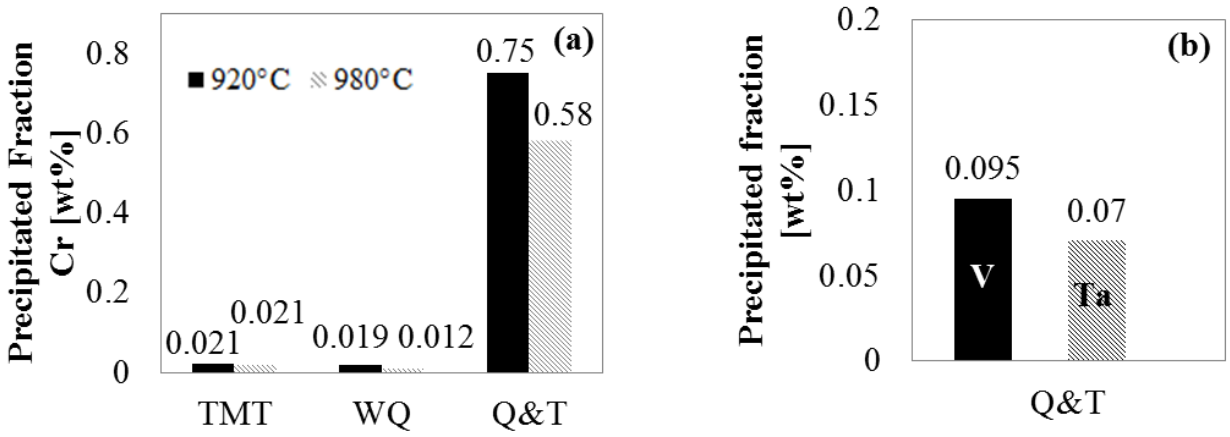

Fig. 6: ICPMS results; (a) Precipitated fraction of Cr after TMT, WQ and Q&T state for annealing temperature of 920°C and 980°C, (b) precipitated fraction of V and Ta in Q&T state with annealing temperature of 920°C. The estimated uncertainty is 0.005 wt%.

By means of ICP-MS, the fraction of Cr-rich $M_{23}C_6$ was quantified, Fig. 6 (a) reveals that only a negligible fraction of 0.019 wt% Cr has precipitated at 920°C. The precipitated Cr fraction in WQ condition after annealing at 980°C is only 0.012 wt%. From this we can deduce that at these annealing temperatures, $M_{23}C_6$ will practically not precipitate during annealing, which is in agreement with the thermodynamic dissolution temperature of 898°C for $M_{23}C_6$ precipitates and

with the presence of $M_{23}C_6$ carbides on block boundaries in Q&T condition after annealing at 920°C, 980°C and 1050°C (Fig. 4).

Additionally, the presence of MX precipitates in WQ condition has been checked with ICP-MS for annealing temperatures of 920°C and 980°C. At these annealing temperatures, a small fraction of (V,Ta)N and TaC is shown to precipitate (Fig. 5 WQ (a) & (b)). The fraction of (V,Ta)N precipitates in WQ condition reduces from 0.021 wt% V to 0.005 wt% V, if the annealing temperature increases from 920°C to 980°C. Comparison between the ICP-MS data at the two annealing temperatures implies that the (V,Ta)N precipitates become unstable at temperatures around 980°C, (Fig. 5 WQ(a) & WQ (b)), which is in full agreement with the thermodynamically calculated dissolution temperature of 987°C for (V,Ta)N precipitates. On the other hand, TaC appears to be stable at 980°C and a similar precipitated fraction of 0.016 - 0.017 wt% Ta is found after annealing at 920°C and 980°C.

On tempering, $M_{23}C_6$ carbides and MX carbonitrides precipitate on grain boundaries and inside the substructure, respectively. ICP-MS results show that precipitation of Cr, V and Ta predominantly occurs during tempering (Fig. 6 (a) Q&T & (b)). In addition, the ICP-OES data revealed that a large fraction of Cr and V remains in solid solution after tempering. Specifically, only 6-8% of the total fraction of Cr in the alloy will precipitate in Q&T condition. In the case of vanadium, 41% of the total fraction of V in the alloy will precipitate in Q&T condition, of which 22% and 5% was formed during annealing at 920°C and 980°C, respectively. For tantalum, 78% of the total amount of Ta in the alloy will precipitate in Q&T condition of which 24% will precipitate during annealing independent of the annealing temperature.

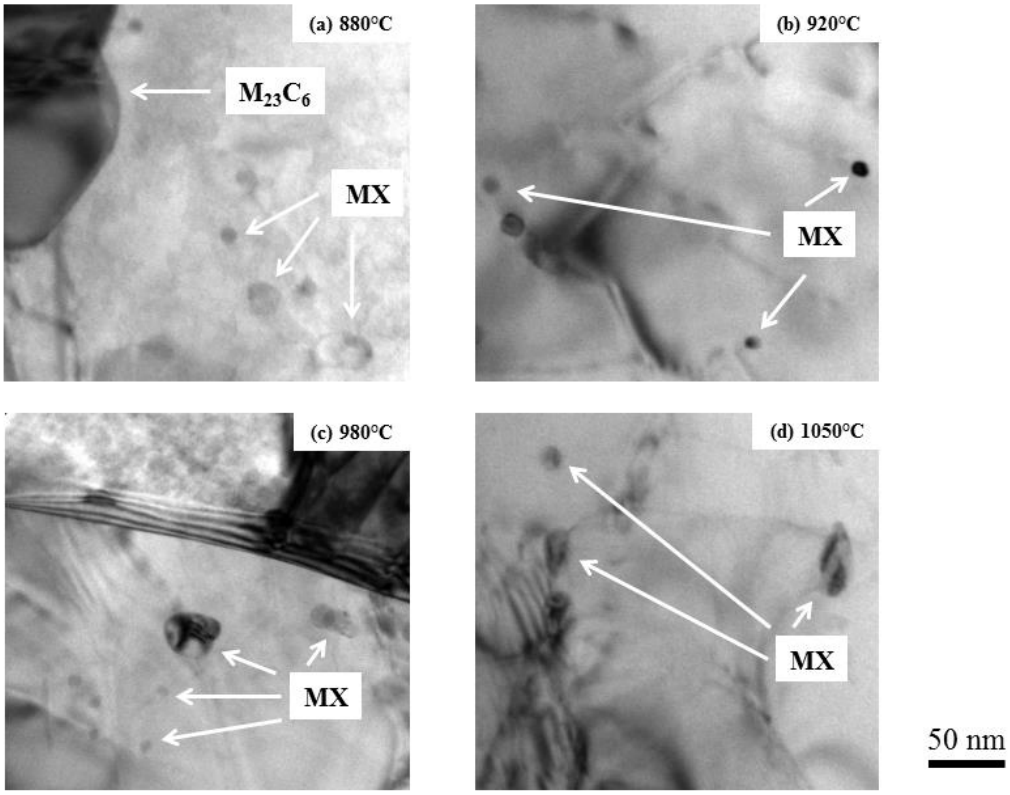

Fig. 7: TEM images of the MX carbonitrides found in the microstructures after Q&T treatments with annealing temperature of (a) 880°C, (b) 920°C, (c) 980°C and (d) 1050°C.

For each sample 10 – 15 TEM micrographs were taken to measure the average diameter of the MX particles. An example for each given Q&T treatment is given in Fig. 7. Quantification of the particle sizes was done by post processing all TEM micrographs with ImageJ software. The average diameter of the MX carbonitrides after tempering as a function of annealing temperature is shown in Fig. 8. Coarser carbonitrides, with average equivalent diameter size of 35 ± 5 nm and 32 ± 4 nm, were observed after tempering for Q(880°C)&T and Q(1050°C)&T treatments, respectively, similar to the previously observed coarser $M_{23}C_6$ carbides obtained by image analysis of SEM microstructures (Fig. 4 (a) & (d)). The average equivalent diameter of the MX carbonitrides after tempering for Q(920°C)&T and Q(980°C)&T is 20 ± 2 nm and 18 ± 2 nm,

respectively. Thus, the particle size is the smallest at an annealing temperature of approximately 950°C.

The size of carbides and carbonitrides in Q&T condition will be dependent on different factors, i.e. available nucleation sites for precipitation during tempering, the fraction of precipitates present in WQ condition and the size of the precipitates formed during annealing. These factors vary with annealing temperature.

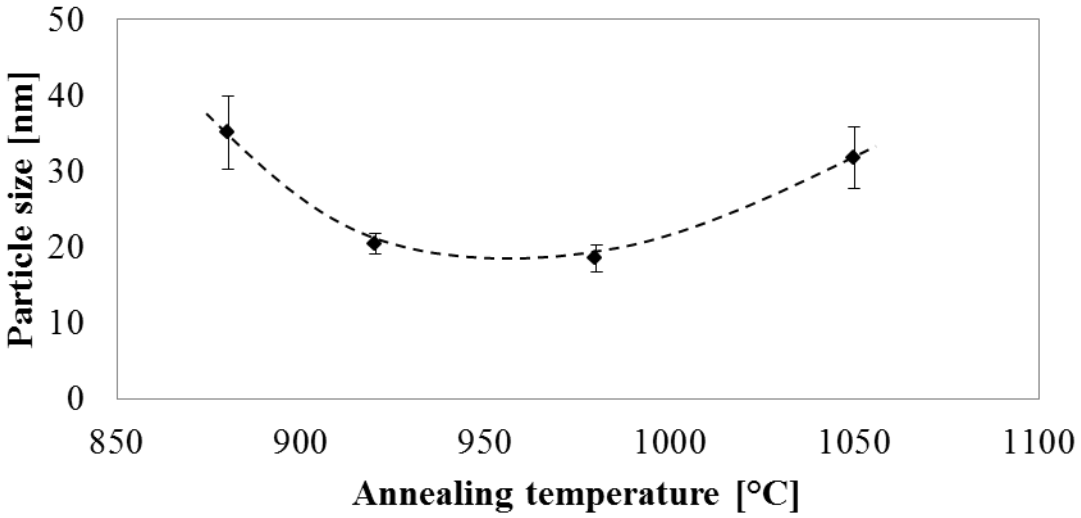

Fig. 8: The average diameter of MX carbonitrides in Q&T condition plotted against annealing temperature, with indicated standard error.

In the case of the $M_{23}C_6$ carbides, the dominant factor affecting the size of the carbides varies depending on the annealing temperature. Specifically, if the annealing temperature is chosen below or above the dissolution temperature. If the annealing temperature is below the dissolution temperature, the $M_{23}C_6$ will precipitate during annealing on the small austenite grains and will coarsen during tempering. On the other hand, if the annealing temperature is chosen above the dissolution temperature, the $M_{23}C_6$ will precipitate during tempering and the size will depend on the amount of available nucleation sites. The nucleation sites for precipitation of $M_{23}C_6$ during

tempering will decrease with increasing block size. As previously discussed, the grain size increases with increasing annealing temperature (Fig. 3), thereby reducing the grain boundary area for the $M_{23}C_6$ to nucleate on. Therefore, with increasing annealing temperature above the dissolution temperature, the size of the $M_{23}C_6$ will also increase. This explains why the biggest $M_{23}C_6$ were seen in the case of Q(880°C)&T and Q(1050°C)&T (Fig. 4).

To explain the trend seen in Fig. 8, the fraction and size of MX particles in WQ condition need to be discussed. As the coarsening rate of MX carbonitrides is typically low due to the slow diffusion of V and Ta at temperatures around 650-750°C [30], the reported size difference must have originated from the annealing step. As discussed, an equal fraction of TaC will be formed at all annealing temperatures, resulting in 24% of the precipitated TaC to be present in WQ condition independently of the annealing temperature. However, as the annealing temperature increases, the amount of Ta, originating from dissolving (V,Ta)N and the amount of C, coming from the dissolved $M_{23}C_6$, in the solid solution will increase. Additionally, as the temperature increases, the diffusion of Ta and C will be facilitated resulting in slightly coarser TaC in WQ condition after annealing at 1050°C. On the other hand, if the annealing temperature is decreased, the fraction of (V,Ta)N that is formed during annealing will increase. These precipitates will be slightly coarsen than the precipitates that form during tempering, as the diffusion of C and N is slower during tempering than during annealing. Summation of the size variations of the two MX particles gives the minimum size of MX particles in Q&T condition after annealing at approximately 950°C (Fig. 8).

3.2 Mechanical properties

The dependence of the hardness on the average martensitic block size in WQ condition is shown in Fig. 9. The hardness of the WQ specimens steadily decreases with increasing block size from

417 ± 5 HV for the material quenched at 880°C to 413 ± 4 HV, 400 ± 4 HV and 390 ± 6 HV for increasing annealing temperatures above A_{c3}: 920°C, 980°C and 1050°C, respectively. The hardness exhibits an inverse relationship with the martensitic block size, while Pavlina *et al.* demonstrated a linear relation between hardness and strength [31]. Therefore, it can be stated that the strength exhibits an inverse relationship with the block size, in accordance with the Hall-Petch relation.

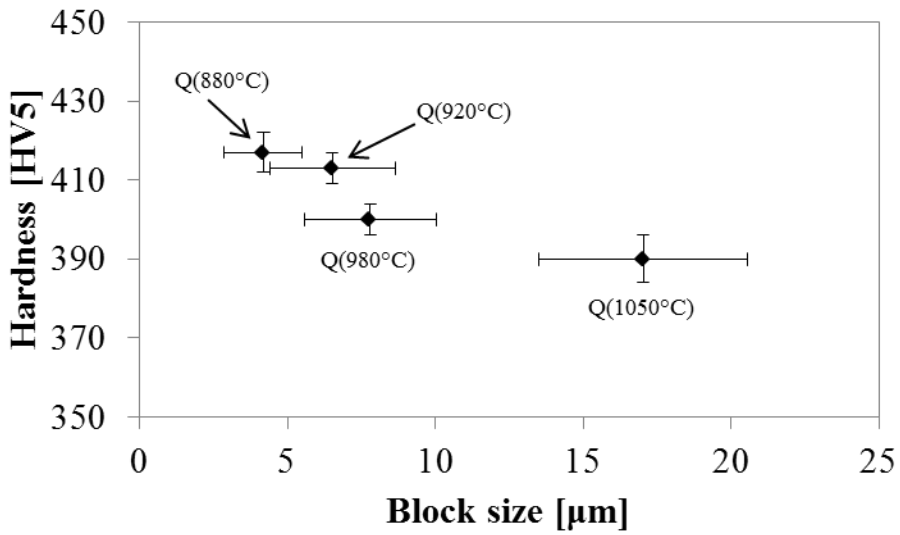

Fig. 9: Vickers hardness measurements of lab-cast EUROFER in different WQ conditions as a function of average martensitic block size with indicated standard error and given annealing treatment.

The loss of hardness after quenching in comparison with the TM-rolled material, i.e. 445 HV, is due to the reduction of defect density in equiaxed austenite during annealing in comparison with the work-hardened austenite after TM-rolling. It was observed by Barani *et al.* [20] that the initial austenitic conditions, in this case the work-hardened austenite during TM-rolling, have significant impact on the properties of the final product phase.

The hardness of the lab-cast EUROFER is lower than the reference EUROFER97-2 when the materials are annealed above $A_{c3,}$ which can be attributed to the different precipitation state of the

reference material. After the conventional hot rolling, applied to the reference material, the initial martensite before annealing is formed in an equiaxed PAG with coarse $M_{23}C_6$ carbides along high angle grain boundaries and needle-shaped MX carbides inside laths and on lath boundaries [29]. If EUROFER97-2 is annealed above A_{c3}, $M_{23}C_6$ and part of the MX precipitates dissolve and reprecipitate dispersively during quenching. This precipitation strengthening explains the higher hardness values of the EUROFER97-2 in comparison with the lab-cast EUROFER annealed at temperatures above A_{c3}. Since, as shown previously, most of the alloying elements in the lab-cast EUROFER are in solid solution in WQ conditions due to TM-rolling, and the contribution of solid solution to the strength is less pronounced than precipitation strengthening.

However, if EUROFER97-2 is reheated below A_{c3}, incomplete dissolution of the coarse $M_{23}C_6$ carbides occurs together with recovery of the martensitic structure. This leads to a softening of EUROFER97-2 in comparison with the fine grained TM-rolled lab-cast EUROFER grade in WQ condition after annealing at 880°C, with almost all alloying elements in solid solution contributing to the solid solution strengthening.

Tensile tests were carried out on the Q&T plate material for the different conditions. The yield strength and ultimate tensile strength at room temperature as a function of the square root of the martensitic block size ($D^{-1/2}$) is given in Fig. 10. An increasing linear trend of the strength levels as a function of the inverse square root of the grain size is observed, as expected according to the Hall-Petch relation. There is, however, a discrepancy between the obtained strength value and the predicted value according to the Hall-Petch relation (Fig. 10) in the case of the smallest grain size, due to the variation of the MX particles sizes with annealing temperature (Fig. 8). The particles formed in Q(880°C)&T are coarser and therefore have a smaller contribution to the

strength. The data thus implies that the precipitation hardening may have dominant effect over the Hall-Petch relation, at the lower annealing temperature.

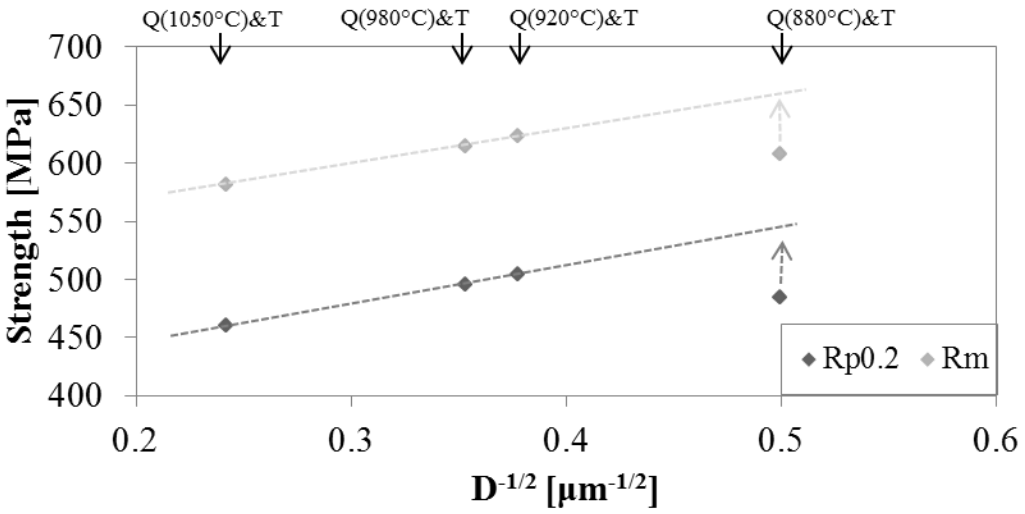

Fig. 10: Ultimate tensile and yield strength as a function of inverse square root of the martensitic block size for lab-cast EUROFER. The standard error of the machine is 1 MPa.

Materna-Morris *et al*. [7] reported yield strength values, obtained with round tensile samples with gauge length of 18 mm and diameter of 3 mm, $R_{p0.2}$ = 543 MPa and ultimate tensile strength R_m = 659 MPa for EUROFER97-2 in conventional Q&T condition [7]. According to F. Hajyakbary, the influence of the specimen geometry on the yield and tensile strength is independent of gauge length [32], consequently the strength values of the reference material can be compared with the lab-cast EUROFER.

Multiple tensile tests were performed in the range of temperatures between -50°C and 850°C to determine the temperature dependence of the strength. The variation of the yield strength for the different Q&T materials with tensile test temperature is shown in Fig. 11.

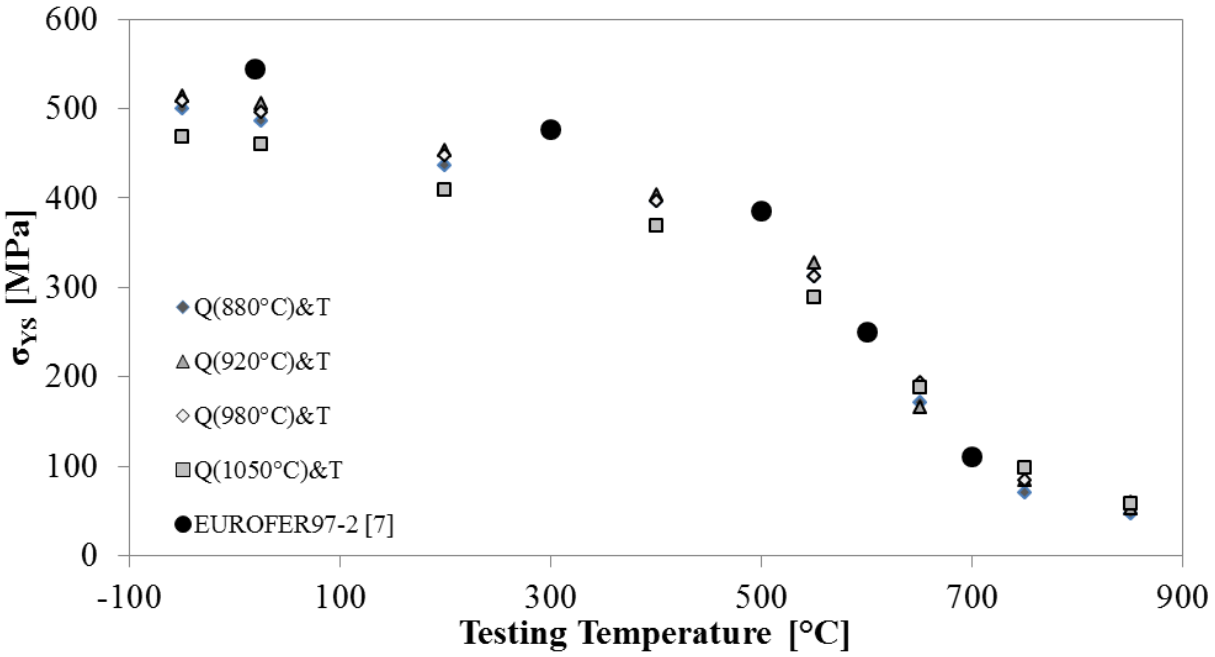

Fig. 11: Yield strength evolution as a function of testing temperature for different Q&T conditions in comparison with EUROFER97-2 [7]. The standard error of the machine is 1 MPa.

Between the different Q&T conditions, a similar decreasing trend with increasing tensile test temperature is observed. The Q(1050°C)&T material exhibits the lowest strength, while the material after a Q(920°C)&T treatment has the highest strength due to grain refinement and a high density of pinning particles. The Q&T materials have a lower strength in comparison with EUROFER97-2. The reduced strength of the Q&T steels is in full agreement with the lower hardness (Fig. 9). At higher temperatures the yield strength levels of the investigated Q&T materials and the reference steel are equivalent. The lab-cast steels exhibit a delay in degradation rate at temperatures above 700°C. No tensile data above 700°C has been reported for EUROFER97-2, so the comparison is not possible in that temperature region. Additionally, the yield strength of the Q(1050°C)&T material appears to be less temperature dependent than the other finer grained Q&T materials. This behaviour is a subject for future studies.

On the contrary, the total elongation of the Q&T materials is higher than that of EUROFER97-2 throughout the tested temperature range as shown in Fig. 12. The mode of crack propagation is intragranular cracking at temperatures below 700°C and intergranular cracking at higher temperatures which explains the loss in ductility around 700°C as also seen by Chauhan *et al*. [33].

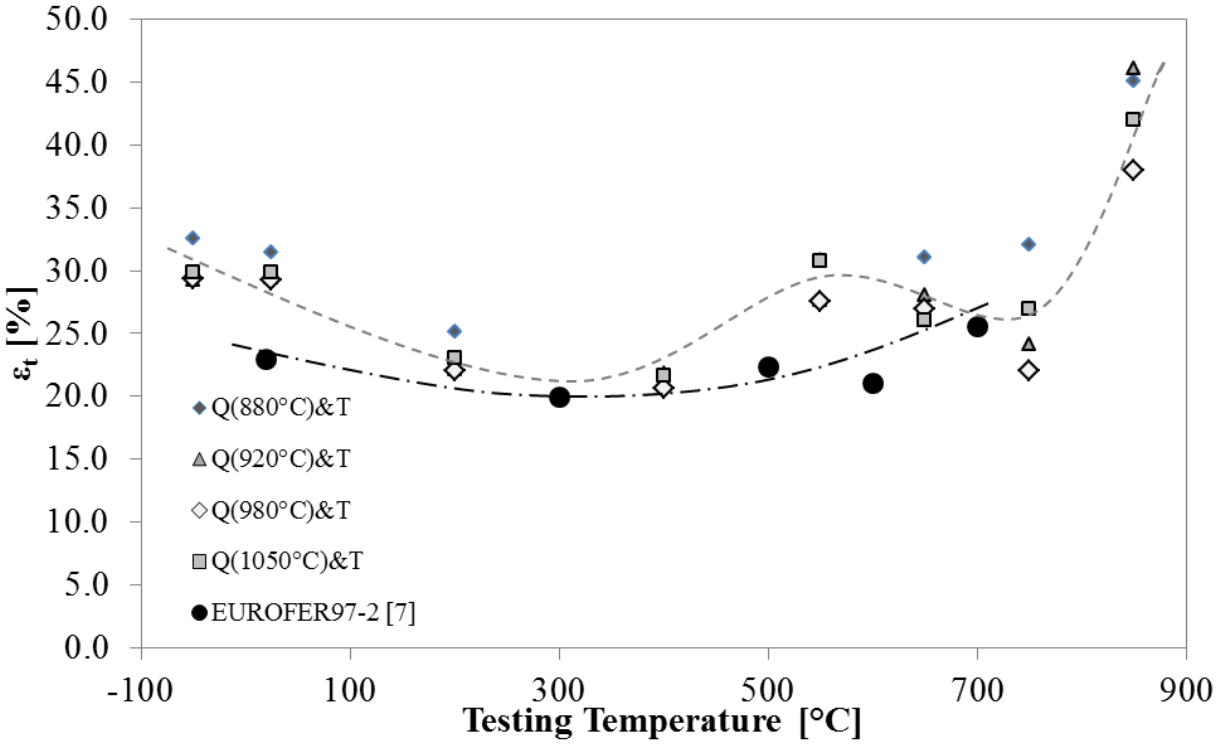

Fig. 12: Total elongation evolution as a function of temperature for different Q&T conditions in comparison with EUROFER97-2 [7]. The standard error for the lab-cast material is 3%.

Charpy V notch impact testing of KLST (Kleinstprobe)-type miniaturized MCVN specimens for a wide temperature window was performed on the Q&T steels to determine the ductile-to-brittle transition temperature (DBTT), the temperature at which the ductile fraction is 50% in the transition zone, and the upper shelf energy (USE). The data of the Q&T material for different annealing temperatures are shown in Fig. 13. The heat treatment with annealing temperature of 880°C has a DBTT of -147°C and a USE of 9.1 J. The DBTT gradually shifts to higher

temperatures of -134°C, -131°C and -109°C with increasing annealing temperature 920°C, 980°C and 1050°C, respectively.

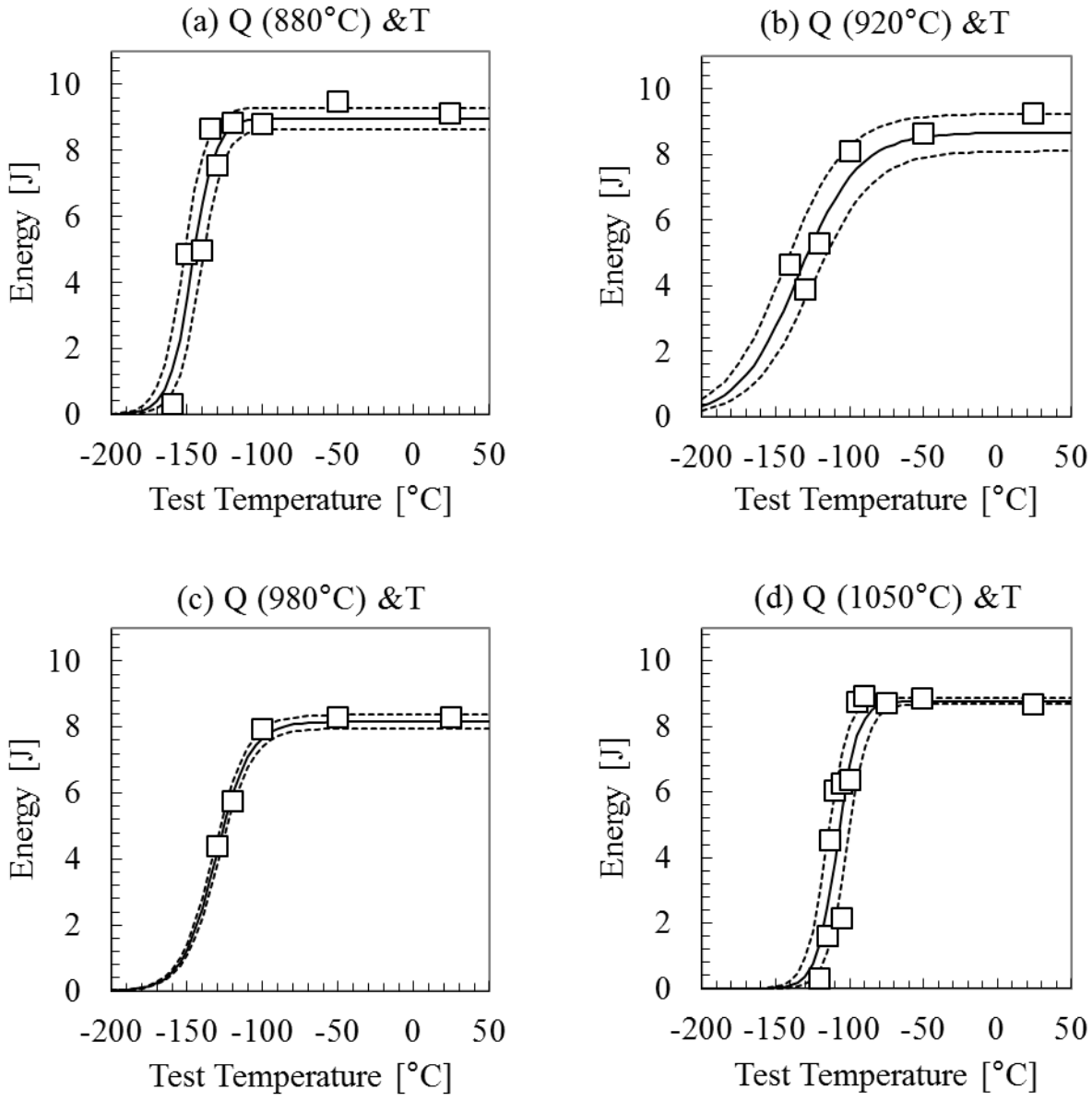

Fig. 13: KLST Charpy results with indicated error bars (dotted lines) for different Q&T conditions.

It is known that refinement of microstructural units of martensite, i.e. packets and block size can improve toughness of martensitic steels [34]. This trend can be confirmed by the impact data represented in Fig. 14. The reported DBTT and USE for KLST tested plate material of Q&T

EUROFER97-2 is -120°C and 9.5 J, respectively [7]. The fact that the DBTT of the lab-cast EUROFER for the Q&T material after annealing at 880°C, 920°C and 980°C is lower in comparison with the reference material confirms the improvement of toughness by applying an alternative processing route.

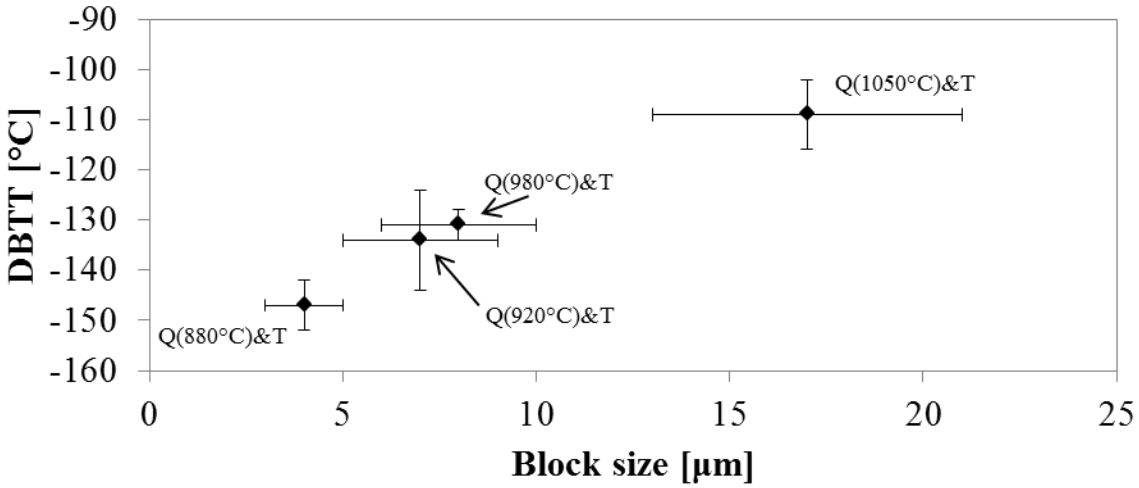

Fig. 14: DBTT as a function of martensitic block size for the lab-cast EUROFER with indicated standard error and given Q&T treatment.

4. Summary and conclusions

In summary, the following statements can be made based on the research on the effect of TM-processing on the microstructure and mechanical properties of the lab-cast EUROFER grade:

- The effects of TM-rolling and micro-alloying with V and Ta lead to alternative precipitation state in comparison with conventionally rolled and heat treated EUROFER97-2. In particular, austenite work-hardening limits precipitation of carbides and carbonitrides after rolling, thereby reducing the final strength of the material and the fraction of precipitates. The size and distribution of the precipitates can be optimized by selecting appropriate annealing temperature.

- TaC precipitates are thermally more stable than (V,Ta)N. Therefore, the Ta content seems to be key for precipitation states that may provide stable mechanical properties at high temperature.
- TM-rolling and Q&T with annealing temperatures up to 980°C lead to a grain refinement of the martensitic structure in comparison with conventionally heat treated EUROFER97-2.
- Adequate adjustments of annealing conditions lead to refined microstructural units of martensite which lower the DBTT of the material.
- The thermo-mechanically treated Q&T materials exhibit better ductility at elevated temperatures, in comparison with EUROFER97-2, while having equivalent toughness and strength values. Nevertheless, the performed experiments do not allow to predict their mechanical behaviour after prolonged exposure to high temperature.

5. Acknowledgments

This work has been carried out within the framework of the EUROfusion Consortium and has received partial funding from the Euratom research and training programme 2014-2018 under grant agreement No 633053. The authors wish to thank the technical staff of the Research Centre OCAS, Zwijnaarde, for the production of the material and the execution of the TM-treatment. The authors also want to thank the mechanical test laboratory of the Belgian Nuclear Research Centre SCK·CEN, Mol for performing the (hot) tensile tests. The views and opinions expressed herein do not necessarily reflect those of the European Commission.

6. References

1. Romanelli, F., *FusionElectricity–A Roadmap to the Realisation of Fusion Energy, European FusionDevelopment Agreement (EFDA), 2012*. ISBN 978-3-00-040720-8.

2. Lucon, E., et al., *The European effort towards the development of a demo structural material: Irradiation behaviour of the European reference RAFM steel EUROFER.* Fusion Engineering and Design, 2006. **81**(8–14): p. 917-923.

3. Tanigawa, H., et al., *Status and key issues of reduced activation ferritic/martensitic steels as the structural material for a DEMO blanket.* Journal of Nuclear Materials, 2011. **417**(1): p. 9-15.

4. Baluc, N., et al., *Status of reduced activation ferritic/martensitic steel development.* Journal of Nuclear Materials, 2007. **367–370, Part A**: p. 33-41.

5. Huang, Q., et al., *Recent progress of R&D activities on reduced activation ferritic/martensitic steels.* Journal of Nuclear Materials, 2013. **442**(1–3, Supplement 1): p. S2-S8.

6. Bornschein, B., et al., *Tritium management and safety issues in ITER and DEMO breeding blankets.* Fusion Engineering and Design, 2013. **88**(6–8): p. 466-471.

7. Materna-Morris, E., et al., *Structural material EUROFER97-2, Characterization of Rod and Plate Material: Structural, Tensile, Charpy and Creep Properties*. 2007, Institut für Materialforschung: Forschungszentrum Karlsruhe. p. 1-88.

8. Aiello, G., et al., *Assessment of design limits and criteria requirements for Eurofer structures in TBM components.* Journal of Nuclear Materials, 2011. **414**(1): p. 53-68.

9. Rieth, M., *The Chemical composition of the EUROFER steel - Historical development, overview, and critical assessment*, I.f.M. I, Editor. 2007: Germany. p. 1-62.

10. Morito, S., Y. Adachi, and T. Ohba, *Morphology and crystallography of sub-blocks in ultra-low carbon lath martensite steel.* Materials transactions, 2009. **50**(8): p. 1919-1923.

11. Morito, S., et al., *The morphology and crystallography of lath martensite in Fe-C alloys.* Acta Materialia, 2003. **51**(6): p. 1789-1799.

12. Klueh, R.L., *Elevated-temperature ferritic and martensitic steels and their application to future nuclear reactors*. 2004, Oak Ridge National Laboratory: Tennessee. p. 1-66.

13. Dossett, J.L. and G.E. Totten, *Steel Heat Treating Fundamentals and Processes*. 2013.

14. Chen, L., et al., *Microstructures and High-Temperature Mechanical Properties of a Martensitic Heat-Resistant Stainless Steel 403Nb Processed by Thermo-Mechanical Treatment.* Metallurgical and Materials Transactions A, 2014. **45**(3): p. 1498-1507.

15. Yoshida, H., et al., *Crystallographic Analysis of Lath Martensite in Ferrite-Martensite Dual Phase Steel Sheet Annealed after Cold-Rolling.* ISIJ International, 2015. **55**(10): p. 2198-2205.

16. Tan, L., et al., *Effect of thermomechanical treatment on 9Cr ferritic–martensitic steels.* Journal of Nuclear Materials, 2013. **441**(1): p. 713-717.

17. Tan, L., Y. Yang, and J.T. Busby, *Effects of alloying elements and thermomechanical treatment on 9Cr Reduced Activation Ferritic–Martensitic (RAFM) steels.* Journal of Nuclear Materials, 2013. **442**(1–3, Supplement 1): p. S13-S17.

18. Thelning, K.E., *Steel and Its Heat Treatment*. 2013: Elsevier Science.

19. Kennett, S.C., *Strengthening and toughening mechanisms in low-c microalloyed martensitic steel as influenced by austenite conditioning*. 2007, Colorado School of Mines. Arthur Lakes Library.

20. Barani, A.A., et al., *Design of high-strength steels by microalloying and thermomechanical treatment.* Materials Science and Engineering: A, 2007. **463**(1): p. 138-146.

21. Ayada, M., et al., *Effect of Vanadium and Niobium on Restoration Behavior after Hot Deformation in Medium Carbon Spring Steels.* ISIJ international, 1998. **38**(9): p. 1022-1031.

22. Yada, H., Y. Matsumura, and K. Nakajima, *Ferritic steel having ultra-fine grains and a method for producing the same*. 1984, Google Patents.

23. Rieth, M., et al., *EUROFER 97 Tensile, Charpy, Creep and Structural Tests*. 2003, Forschungszentrum Karlsruhe: Germany.

24. Prat, O., et al., *The role of Laves phase on microstructure evolution and creep strength of novel 9%Cr heat resistant steels.* Intermetallics, 2013. **32**(0): p. 362-372.

25. Rojas, D., et al., *9%Cr heat resistant steels: Alloy design, microstructure evolution and creep response at 650°C.* Materials Science and Engineering: A, 2011. **528**(15): p. 5164-5176.

26. Sonderegger, B., S. Mitsche, and H. Cerjak, *Microstructural analysis on a creep resistant martensitic 9–12% Cr steel using the EBSD method.* Materials Science and Engineering: A, 2008. **481–482**(0): p. 466-470.

27. Standard, A., *E8/E8M, 2013a," Standard Test Methods for Tension Testing of Metallic Materials," ASTM International, West Conshohocken, PA, 2013, DOI: 10.1520/E0008_E0008M*.

28. Rudnev, V., et al., *Handbook of Induction Heating*. 2002: CRC Press.

29. Chandravathi, K.S., et al., *Effect of isothermal heat treatment on microstructure and mechanical properties of Reduced Activation Ferritic Martensitic steel.* Journal of Nuclear Materials, 2013. **435**(1–3): p. 128-136.

30. Mythili, R., et al., *Microstructural Modifications Due to Tungsten and Tantalum in 9Cr Reduced Activation Ferritic Martensitic Steels on Creep Exposure.* Procedia Engineering, 2013. **55**: p. 295-299.

31. Pavlina, E. and C. Van Tyne, *Correlation of yield strength and tensile strength with hardness for steels.* Journal of Materials Engineering and Performance, 2008. **17**(6): p. 888-893.

32. Hajyakbary, F., *Optimising mechanical behaviour of new advanced steels based on fine non-equilibrium microstructures*. 2015, TU Delft, Delft University of Technology.

33. Chauhan, A., D. Litvinov, and J. Aktaa, *High temperature tensile properties and fracture characteristics of bimodal 12Cr-ODS steel.* Journal of Nuclear Materials, 2016. **468**: p. 1-8.

34. Morris, J., JW, et al., *Advances in Physical Metallurgy and Processing of Steels. The Limits of Strength and Toughness in Steel.* ISIJ international, 2001. **41**(6): p. 599-611.

List of Tables

Table 1: Chemical composition of EUROFER97-2 [7] and lab-cast EUROFER grade.

[wt%]	C	Si	Mn	P	S	N	V	Ta	W	Cr	Fe
EU97-2	0.09-0.12	0.05	0.2-0.6	0.005	0.005	0.015-0.045	0.15-0.25	0.10-0.14	1-1.2	8.5-9.5	Bal.
Lab-cast EUROFER	0.11	0.038	0.40	0.0023	0.0029	0.011	0.22	0.086	1.0	9.3	Bal.

List of Figures

Fig. 1: Schematic representation of the TM rolling followed by air cooling (TMT) and heat treatment with variable T_{anneal} =880°C, 920°C, 980°C and 1050°C for 30 min. followed by water quenching (WQ) and tempering at 750°C for 2 hrs. (Q&T).

Fig. 2: Unique grain color maps in WQ conditions with annealing temperature of (a) 880°C, (b) 920°C, (c) 980°C and (d) 1050°C.

Fig. 3: Black symbols: average martensite block size measurements obtained via orientation imaging microscopy (OIM^{TM}) data analysis for lab-cast EUROFER, with standard error, compared with grain size data available for EUROFER97-2 given by the grey symbols [7].

Fig. 4: SEM images of material in Q&T condition after different annealing temperatures (a) 880°C, (b) 920°C, (c) 980°C and (d) 1050°C.

Fig. 5: ICPMS results; fraction of MX precipitates after TMT and as-quenched (WQ) for annealing temperature of 920°C (a) and 980°C (b). The estimated uncertainty is 0.005 wt%.

Fig. 6: ICPMS results; (a) Precipitated fraction of Cr after TMT, WQ and Q&T state for annealing temperature of 920°C and 980°C, (b) precipitated fraction of V and Ta in Q&T state with annealing temperature of 920°C. The estimated uncertainty is 0.005 wt%.

Fig. 7: TEM images of the MX carbonitrides found in the microstructures after Q&T treatments with annealing temperature of (a) 880°C, (b) 920°C, (c) 980°C and (d) 1050°C.

Fig. 8: The average diameter of MX carbonitrides in Q&T condition plotted against annealing temperature, with indicated standard error.

Fig. 9: Vickers hardness measurements of lab-cast EUROFER in different WQ conditions as a function of average martensitic block size with indicated standard error and given annealing treatment.

Fig. 10: Ultimate tensile and yield strength as a function of inverse square root of the martensitic block size for lab-cast EUROFER. The standard error of the machine is 1 MPa.

Fig. 11: Yield strength evolution as a function of testing temperature for different Q&T conditions in comparison with EUROFER97-2 [7]. The standard error of the machine is 1 MPa.

Fig. 12: Total elongation evolution as a function of temperature for different Q&T conditions in comparison with EUROFER97-2 [7]. The standard error for the lab-cast material is 3%.

Fig. 13: KLST Charpy results with indicated error bars (dotted lines) for different Q&T conditions.

Fig. 14: DBTT as a function of martensitic block size for the lab-cast EUROFER with indicated standard error and given Q&T treatment.